Investigation on the wind preview quality for lidar-assisted wind turbine control under wake conditions

Feng Guo[1,2*], David Schlipf[1], Zhaoyu Zhang[3], Po Wen Cheng[2]

***Abstract*— The wind preview provided by a nacelle-based lidar system allows the wind turbine controller to react to the wind disturbance prior to its impact on the turbine. This technology, commonly referred to as lidar-assisted wind turbine control, has been shown to be beneficial in reducing wind turbine structural loads. The wind preview quality defines how the lidar estimated disturbance is correlated with the actual one. In practice, the preview quality can vary following the change in atmospheric conditions and lidar operating states.**

When assessing the benefits of lidar-assisted control, previous studies mainly focused on the freestream turbulence where the turbine wake has not been included. In reality, wind turbines sometimes operate within the wake caused by upstream situated turbines, which happens more often in a narrowly spaced wind farm. Based on existing literature, the wake turbulence has three main phenomena compared with the freestream turbulence, i.e. (1) the reduced wind speed region (wake deficit), (2) the meandering (wake deficit moves in the lateral and vertical directions), and (3) the smaller-scale added turbulence caused by the interaction between rotor and the flow. The extent to which these phenomena affect the quality of lidar wind preview still needs to be investigated.

In this paper, we use the dynamic wake meandering model, which covers the three wake characteristics mentioned above, and analyze its impact on lidar wind preview qualities. The most representative turbine layout where two turbines lie in a row will be considered. Frequency-domain analysis will be carried out to assess the measurement coherence of the lidar and the results will be compared to the freestream case.

I. INTRODUCTION

Lidar-assisted control (LAC) utilizes the lidar upstream wind preview measurement and allows the turbine to pre-act to the incoming disturbance [1], [2]. However, lidar system does not provide perfect measurement mainly due to the limited measuring positions, the contamination by lateral and vertical wind components, and the evolution of turbulence [3], [4], [5]. The wind preview quality is defined to describe how the lidar preview is correlated with the actual rotor effective wind speed (REWS) experienced by the turbine [6].

Previous research mainly concentrated on studying the lidar wind preview for control in the freestream turbulence situation [7], [3], [8]. In this context, the turbulence is assumed to be homogeneous and Gaussian which can be modelled using the Mann uniform shear model [9] or the Kaimal spectra and exponential coherence model [10] (hereafter refereed as to Mann model and Kaimal model respectively). These two models are provided by IEC-61400:2019 [11] for wind turbine design under freestream turbulence situation.

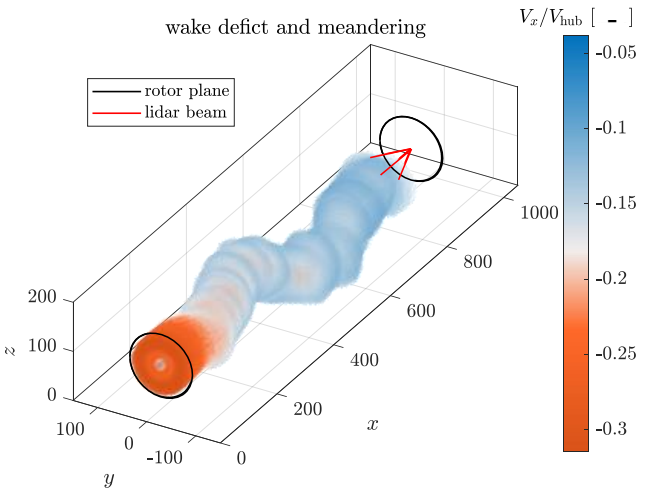

Fig. 1. Sketch of the meandering wake deficit for a downstream turbine and a lidar system. V_x denotes the mean longitudinal wind speed deficit in the wake and V_{hub} is the freestream hub height mean wind speed.

Three main characteristics present in the turbine wakes [11], [12], i.e. (1) the reduced wind speed region (wake deficit), (2) the meandering (wake deficit moves in the lateral and vertical directions), and (3) the smaller-scale added turbulence caused by the interaction between rotor and the flow. Based on these phenomena, one can conceive possible impact on lidar wind preview caused by the wake. For example, the wake is measured by a lidar in an upstream yz plane, as sketched in Figure 1. Then it propagates (in x-direction) to the turbine with meandering so that the sectional overlap of the wake at the rotor disk changes in time. When the wake reaches the rotor plane, it might be partly overlapped with the rotor; miss the rotor entirely; or become less important due to wake recovering. These can cause additional errors between the lidar estimated REWS and that by the rotor.

The lidar preview quality under wake conditions has not been fully explored in literature. Thus, we contribute by studying the impact of wake on lidar preview quality in the frequency domain. The Mann uniform shear model [13] will be combined with the Dynamic Wake Meandering model (DWM), both suggested by IEC standard [11] to model wake turbulence. We perform the analysis using different turbulence parameters that represent various atmospheric

[1]Wind Energy Technology Institute, Flensburg University of Applied Sciences, Kanzleistraße 91–93, 24943 Flensburg, Germany feng.guo@hs-flensburg.de

[2]Stuttgart Wind Energy (SWE), Institute of Aircraft Design, University of Stuttgart, Allmandring 5b, 70569 Stuttgart, Germany

[3]Department of Mechanical Engineering, Politecnico di Milano, via La Masa 1, 20156 Milano, Italy

TABLE I

SCAN CONFIGURATION FOR THE SELECTED LIDAR SYSTEM.

number of beams n	4
beam azimuth-angles ϕ [°]	15.0, 15.0, -15.0, -15.0
beam elevation-angles β [°]	12.5, -12.5, -12.5, 12.5
measurement distance	120 m
full scan time	1.0s
pulse width at half maximum	30 m

TABLE II

THE MANN PARAMETERS OF DIFFERENT ATMOSPHERIC STABILITIES.

	$\alpha\varepsilon^{2/3}$ [$\mathrm{m}^{4/3}\mathrm{s}^{-2}$]	Γ [-]	L [m]
Unstable (u)	0.06	2.6	142
Neutral (n)	0.11	3.5	55
Stable (s)	0.09	2.9	26

stabilities and consider several wind direction scenarios.

This paper is structured as follows: Section II describes the selected turbine and lidar model as well as introduces the method to simulate wake included wind fields. Also, the calculation of lidar measurement and rotor effective wind speed are discussed. In Section III, the simulation set-up is discussed and the results are shown. Finally, we conclude the paper and discuss perspective further works in Section IV.

II. SIMULATION ENVIRONMENT

In this section we present the simulation environment used in this work. We first define the studied lidar system and wind turbine. Then we describe the used freestream turbulence model and the simulation of the wake included turbulence field. The simulation of the lidar measurements and the calculation of the lidar wind preview quality are described in the end.

A. Lidar System and Wind Turbine Model

We consider the scan trajectory based on a typical commercial lidar system, whose configurations are summarized in Table I. As for the turbine model, the 5MW reference wind turbine by NREL [14] is considered, which has a rotor diameter of $126\,\mathrm{m}$ and a hub height of $90\,\mathrm{m}$.

B. Freestream Turbulence Model

The Mann model [13] is chosen in this work. It is derived based on the linearized Navier-Stokes (N-S) equations assuming incompressible flow and it includes the spatial coherence of lateral (v) and vertical (w) wind components. Since the wake meandering that will be introduced later is driven by the lateral and vertical wind components, we think these physical considerations are important for simulating the meandering of the wake. Moreover, there are existing studies that relate Mann model [9] parameters to atmospheric stabilities using measurement data [15]. This supports us to perform the analysis under different atmospheric stabilities.

In Mann model [9], the fluctuation part of the turbulence is described by the spectral tensor:

$$\mathbf{\Phi}_{ij}(\boldsymbol{k})\delta(\boldsymbol{k}-\boldsymbol{k'}) = \langle \hat{u}_i^*(\boldsymbol{k})\hat{u}_j(\boldsymbol{k'})\rangle, \tag{1}$$

where $\langle\ \rangle$ denotes ensemble average, * denotes the complex conjugate, $\delta()$ is the Dirac delta function, $\boldsymbol{k}$= (k_1, k_2, k_3) (or $\boldsymbol{k'}$) is the wavenumber vector. The $\boldsymbol{k'}$ used here is to distinguish the case: $\boldsymbol{k}\neq\boldsymbol{k'}$. $\hat{u}_i$ or $\hat{u}_i$ are the Fourier coefficients after taking the three dimensional Fourier transform of the velocity components $u_i(x, y, z)$. The indexes $i, j = 1, 2, 3$ stand for u, v, and w components. The detailed calculation of the tensor $\mathbf{\Phi}_{ij}$ can be found in [9]. Apart from the wavenumber vector, there are three other parameters in the model. They are the energy level constant $\alpha\varepsilon^{2/3}$, the length scale L describing the size of the eddies containing the most energy [3], and the non-dimensional anisotropy Γ describes the extent of shear distortion that causes anisotropic turbulence. When $\Gamma = 0$, the turbulence is isotropic [13], [16], which means all velocity components have identical statistical properties. In practice, the parameter $\alpha\varepsilon^{2/3}$ is scaled to adjust the turbulence intensity.

In the result of this paper, we use three Mann parameter sets based on the study by [15], which represent three atmospheric stabilities, see Table II for detail. These parameters are derived by fitting the measurement data from a 250m tall mast tower at the Østerild wind turbine test station in northern Denmark to the Mann model [13]. The parameters related to the 103m height which is close to the hub height of the studied reference turbine (90m) are used.

C. Wake Included Turbulence Modelling

In this section, we explain the three sub-modules of the DWM model and show how they are combined to simulate the wake included turbulence field.

1) Wake deficit: As recommended by [11], the wake deficit is modelled using the thin layer approximation of the N-S equations in their rotational symmetric form disregarding the pressure term [11], [17]. And the eddy-viscosity formulation is used for turbulence closure [18]. The mean wake velocities in longitudinal direction V_x and that in radial direction V_r are governed by the momentum equation:

$$V_x\frac{\partial V_x}{\partial x} + V_r\frac{\partial V_x}{\partial r} = \frac{1}{r}\frac{\partial}{\partial r}\left(r\nu_T\frac{\partial V_x}{\partial r}\right), \tag{2}$$

and the continuity equation:

$$\frac{1}{r}\frac{\partial}{\partial r}(rV_r) + \frac{\partial V_x}{\partial x} = 0. \tag{3}$$

Both V_x and V_r are functions of radial (r) and longitudinal (x) displacements from the wake center. The IEC standard [11] suggests an expression for the eddy viscosity ν_T which only depends on x. In this paper, we use the eddy viscosity formulation implemented within FAST.Farm [18], which depends on both r and x. Because several studies have been performed to validate the FAST.Farm either using Large Eddy Simulation or measurement data [19], [20]. In our implementation, the wake deficit are calculated following: 1)

obtain steady-state axial induction factors and thrust coefficients of blade elements from aeroelastic tool OpenFAST[1]; 2) deliver freestream turbulence parameters and calculate eddy viscosity; 3) solve equation (2) and (3) using the finite-difference method discussed by [18].

2) Wake meandering: The wake meandering is modelled by considering it acting as passive tracers [11]. With Taylor's hypothesis [21], the deficits transport downstream by the mean ambient longitudinal wind field [17]. At a given moment, the wake center coordinate (y_c,z_c) is assumed to be driven by the large-scale lateral and vertical velocity fluctuations v_c and w_c [22], [12], which can be formulated as

$$\dot{y}_c(x) = v_c(x) = \frac{1}{\pi R_w^2}\iint_D v(x,y,z)\mathrm{d}y\mathrm{d}z, \tag{4}$$

$$\dot{z}_c(x) = w_c(x) = \frac{1}{\pi R_w^2}\iint_D w(x,y,z)\mathrm{d}y\mathrm{d}z, \tag{5}$$

where the integration area D is the wake cross-section area. This spatial average of the fluctuations within the wake plane results in the following auto-spectrum of the averaged fluctuation:

$$S_{R,ii}(k_1) = \iint_{-\infty}^{\infty} \Phi_{ii}(\boldsymbol{k})\frac{4J_1^2(\kappa R_w)}{\kappa^2 R_w^2}\mathrm{d}k_2\mathrm{d}k_3, \tag{6}$$

with $\kappa = \sqrt{k_2^2+k_3^2}$, J_1 the Bessel function of the first kind [3], and the index numbers i,j standard for v_c and w_c respectively. Because the auto-spectrum of single point is simply $F_{ii} = \int_{-\infty}^{\infty}\Phi_{ii}(\boldsymbol{k})\mathrm{d}k_2\mathrm{d}k_3$, it leads to the following low pass filtering gain:

$$G_{Ri}(k_1) = \left(\frac{S_{R,ii}(k_1)}{F_{ii}(k_1)}\right)^{\frac{1}{2}}. \tag{7}$$

It is worth mention that the spatial filtering by Equation (7) is only for the initial wake center movement behind the rotor. For wake planes further downstream, the position of the wake cross-section is continuously changing, therefore the integration area D is time-dependent and the filtering gain does not have a simple expression. As suggested by [22], [11], a reference low-pass filter with a cut-off frequency of $V_{hub}/4R_w$ is further applied to v_c and w_c. Figure 2 shows the gain of the spatial filtering under different atmospheric stabilities and the gain of the low pass filter. It is clear that the stable condition with smaller turbulence length scale has stronger filtering effect. Note that the wavenumber is converted to frequency by $k_1 = 2\pi f/V_{hub}$ with Taylor's frozen theory [21], [23].

3) Wake induced turbulence: The wake induced turbulence is mainly originated from the mechanical interaction between the turbine blade and the wind flow [11]. We follow the recommended modelling procedure by the IEC standard [11] where the wake induced turbulence meanders with the deficit and it is independent from the freestream turbulence. Also, the wake induced turbulence is approximated by scaling an isotropic turbulence field whose length scale is smaller than or equal to the rotor diameter [11]. When used with Mann model [9], the isotropic turbulence field is assumed to has a length scale equals to 25% of the ambient turbulence length scale [12], [17]. The empirical calling factor [11] is calculated by

$$k_{wt}(x,r) = 0.6\left|1-\frac{V_x+V_{hub}}{V_{hub}}\right| + \frac{0.35}{V_{hub}}\left|\frac{\partial V_x}{\partial r}\right|. \tag{8}$$

The implementation of the DWM model is shown in Figure 3. The steady state wake deficit and the induced wake scaling factor can be firstly calculated. But the wake meandering needs to be calculated dynamically in the simulation. Adopting the Taylor's hypothesis [21], the freestream turbulence propagates by the mean ambient wind speed. In each time step, the wake deficit field $V_x(x,y,z)$ and induced turbulence field $\hat{u}_{i,w}(x,y,z)$ are calculated and added to

[1]https://github.com/OpenFAST/openfast, last access: Sep. 2021, National Renewable Energy Laboratory

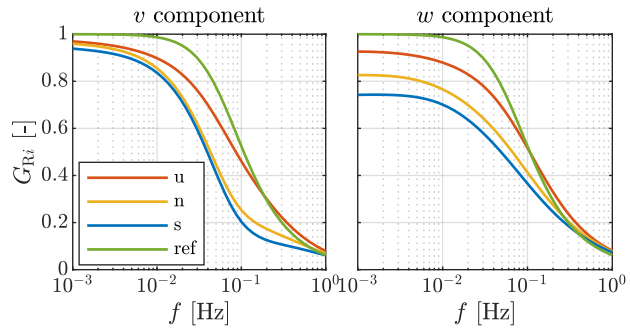

Fig. 2. The spatial filtering gains with Mann parameters listed in Table II and the reference low-pass filter gain (V_{hub} = 16 m/s, R_w =63 m).

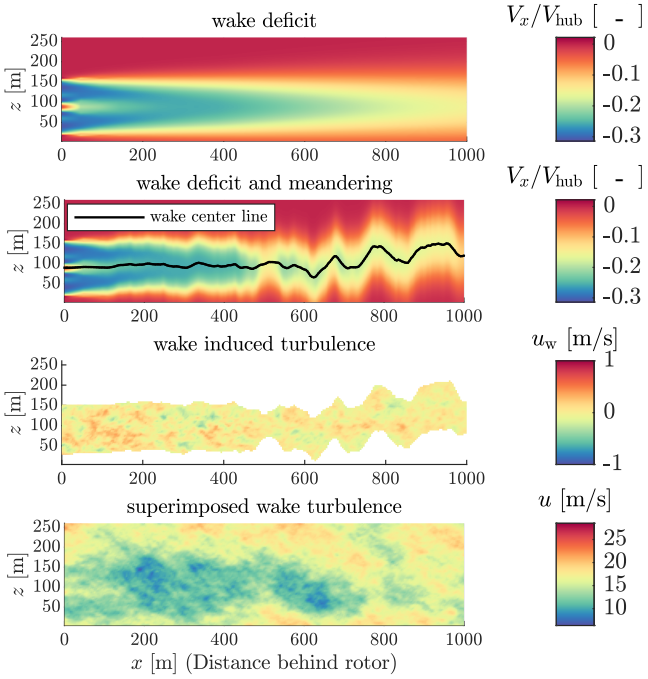

Fig. 3. Side view of the wake characteristics and the wake included turbulent wind field with a hub height mean wind speed of 16 m/s. As for the wake induced turbulence, the points outside the wake area are not plotted.

the freestream turbulence field $u_i(x, y, z)$. The freestream turbulence is generated using *Mann turbulence generator*[2], made available by Technical University of Denmark.

D. Rotor effective wind and lidar preview quality

Similar to [24], [8], the REWS for control purpose is approximated by the mean longitudinal wind speed over the rotor area (denoted by D), i.e.

$$u_{\mathrm{R}}(t) = \frac{1}{\pi R^2} \iint_D u(t, y, z) \mathrm{d}y \mathrm{d}z. \tag{9}$$

To calculate the lidar estimated REWS u_{L}, the lidar line-of-sight (LOS) measurement first needs to be defined. The typical modelling approach in literature is adopted where the LOS is approximated by the weighted sum of radial wind speeds along the lidar beam [24], [8]:

$$v_{\mathrm{los}} = \int_{-\infty}^{\infty} (x_{\mathrm{n}} u(s) + y_{\mathrm{n}} v(s) + z_{\mathrm{n}} w(s)) f_{\mathrm{RW}}(s) \mathrm{d}s, \tag{10}$$

where s denotes the displacement distance from the focused position, $f_{\mathrm{RW}}(s)$ is the weighting function and $[x_{\mathrm{n}}, y_{\mathrm{n}}, z_{\mathrm{n}}] = [\cos\beta\cos\phi, \cos\beta\sin\phi, \sin\beta]$ is the unit vector reflecting the projection from wind velocity components to the LOS direction. The unit vector can be simply calculated after knowing the lidar beam trajectory defined by the azimuth angle ϕ and elevation angle β. For the pulsed lidar used in this work, the weighting function is modelled by a Gaussian-shape function, see [25] for more detail. Following [25], [6], the lidar estimated REWS is calculated by

$$u_{\mathrm{L}}(t) = \frac{1}{x_{\mathrm{n}}} \frac{1}{n} \sum_{j=1}^{n} v_{\mathrm{los},j}(t), \tag{11}$$

where n is the number of lidar focused positions.

With u_{R} and u_{L}, it is common to assess the frequency-domain correlation by calculating the coherence γ_{RL} of these two signals [25], [23]. However, in LAC application, another indication of how well the lidar predict the REWS is by the transfer function below [25], [26]:

$$|G_{\mathrm{RL}}(f)| = \frac{|S_{\mathrm{RL}}(f)|}{S_{\mathrm{LL}}(f)}, \tag{12}$$

where $|S_{\mathrm{RL}}(f)|$ is the absolute value of the cross-spectrum between u_{R} and u_{L} and $S_{\mathrm{LL}}(f)$ is the auto-spectrum of u_{L}. They both could be estimated by the Fourier transform of the target signals. The transfer function can be interpreted as an optimal Wiener's filter [26], [27], which ideally gives the minimal variance of the turbine dynamic output when lidar-assisted feedforward control is implemented. For a certain frequency, the larger gain means that more information from lidar measurement can be utilized as control input. Therefore, we compare the lidar preview quality under wake conditions by assessing the optimal filter gains in the rest of the paper. In the case of freestream turbulence, the theoretical transfer function gain has been derived in [23].

[2]https://www.hawc2.dk/Download/Pre-processing-tools/Mann-64bit-turbulence-generator, last access: 20 Dec 2020

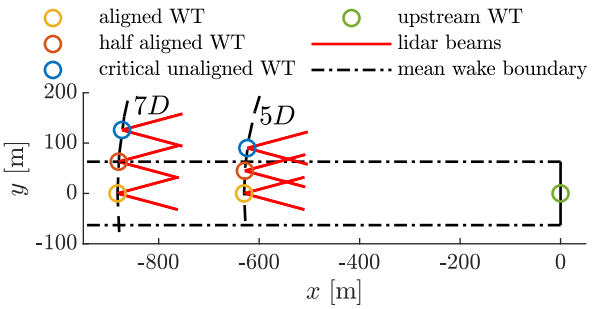

Fig. 4. Top view of the the considered turbine layout. For both 7D and 5D separations, three different aligning conditions correspond to different wind directions are considered.

III. SIMULATION AND RESULTS

For the simulation set-up, we consider the layout that two turbines align in a row with the typical 5D and 7D (D is the rotor diameter) spacing. Three wind directions are considered to simulate partial and full wake cases for the downstream turbine. As shown by Figure 4, we define three wind directions based on the 7D separation. The full wake case corresponds to that the 7D downstream turbine is aligned with the upstream turbine and the wind direction; the half aligned means that half of the turbine rotor at 7D is in the mean wake boundary; and the critical non-aligned stands for that the turbine is just outside the wake boundary. For the 5D case, the downstream turbine is moved towards the upstream turbine by 2D along the line between the 7D position and the upstream turbine. The Mann parameters listed in Table II are used to simulate various atmospheric stabilities, as for the $\alpha\varepsilon^{2/3}$, it is adjusted to meet the target reference turbulence intensity.

For each simulation configuration, we apply the Monte Carlo method [28] using 12 different random seeds to generate the turbulence fields. A wake included turbulence field with the dimensions $8192\times64\times64$ and the resolutions $4\,\mathrm{m} \times 6.1\,\mathrm{m} \times 6.1\,\mathrm{m}$ in x, y and z directions is simulated. With Taylor's frozen theory [21] applied, each field has a total simulation time of $2048\,\mathrm{s}$. For comparison, the same turbulence field but without wake are used to calculate lidar- and turbine- based REWS in the wake-free scenario. The mean hub height wind speed of $16\,\mathrm{m/s}$ and the reference turbulence intensity of 0.16 are considered. The simulated time series are collected and detrended by the mean value. Then the spectra are calculated using Welch's method [29] with hamming windows (size of 2048 data points).

The results of REWS time series from one simulation by the "5D aligned" configuration in unstable atmosphere are chosen as an example and shown in Figure 5. By comparing (a) with (b), it can be seen that the wake deficit causes lower mean values in (a) than that in (b). The mean u_{L} is slightly lower than the mean u_{R} in (a) because of the wake recovering. But the difference is relatively small. In (c), the difference of RWESs in the wake-included and in the freestream cases are compared. The fluctuation in the difference is much smaller than the ambient turbulence

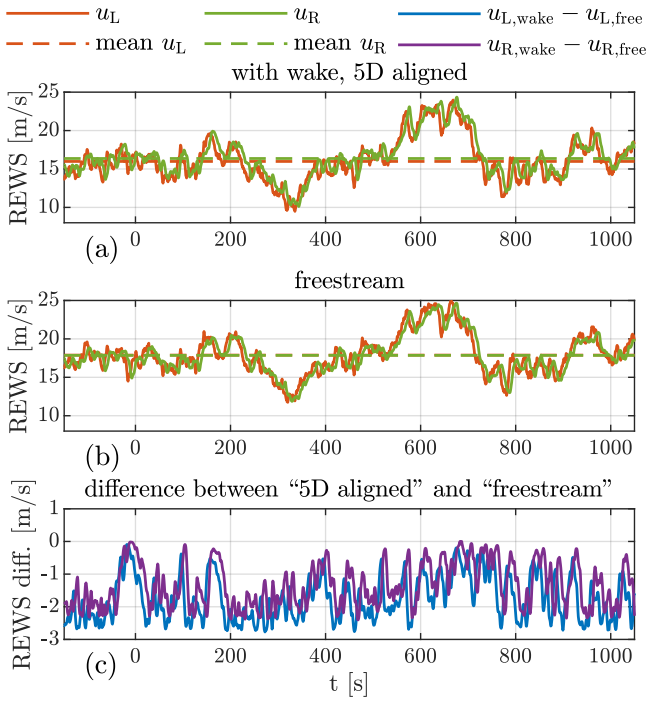

Fig. 5. Time series of the simulated REWSs.

fluctuation. Overall, the lidar preview shows good agreement with the turbine-based REWS in both wake-included and freestream scenarios.

The results of spectra estimations of u_L are shown in Figure 6. The agreements between the theoretical $S_{LL}(f)$ and that by the simulated time series validate the simulation results. Comparing the wake included $S_{LL}(f)$ with that of freestream, there are mainly some additional variances (area below the $f \cdot S$ curve) in frequency range 0.01 Hz to 0.02 Hz in the aligned layout. The auto-spectra of the additional fluctuations ($u_{L,wake} - u_{L,free}$) introduced by the wakes are also shown, which are much smaller than that caused by the ambient turbulence. Overall, we find that adding the DWM model does not have a significant impact on the spectral proprieties of the lidar measurement. Also, the stable turbulence with smaller length scale L shows less variance of the lidar estimated REWS due to the stronger spatial averaging effect than neutral and unstable conditions.

The results of the optimal filter gain are shown in Figure 7. Here, only the "aligned" and the "critical unaligned" cases are shown to keep the readability of the figure. Based on the previous discussion on the spectra, as expected, the filter gain is not influenced considerably by adding the wake effect described by DWM model. By comparing the transfer functions in different stabilities, the main difference is that the larger length scale from the unstable case has a higher cut-off frequency (the frequency where the gain cross -3 dB), which means more frequency components could be used for LAC. In the unstable case, we can see the transfer function gain is slightly better than that of the theoretical freestream case, which might be caused by the additional coherent turbulence structure (see Figure 5 c) added by the wake effect.

IV. CONCLUSIONS AND OUTLOOKS

In this work, we implement the Dynamic Wake Meandering (DWM) model to simulate wake included turbulent wind fields. The wake included wind field is generated by combining the freestream Mann turbulence [16] and the wake characteristics described by DWM model. The DWM model is combined by the wake deficit, the wake meandering, and the wake induced turbulence.

We implement the lidar simulation into the wake included turbulent field and assess the lidar preview quality under various conditions. We considered turbulence parameters representing different atmospheric stabilities, different spacing between downstream and upstream turbines, and different wind directions corresponding to different wake exposure scenarios.

Overall, the simulation result shows that the wake described by DWM model has neglectable impact on the lidar preview quality. The preview quality under different turbine separations and directions in the wake conditions is similar to that in the freestream, and the frequency results from simulations show good agreement with the theoretical curves derived from Mann model [13].

The DWM model is however not solving the turbulent flow physically. In future work, higher fidelity wake solutions, such as the Large Eddy Simulation (LES) based approach, could be applied to verify the DWM model on lidar preview quality estimation. In addition, the temporal delay effect caused by the wake, that is not addressed in this work, can be further studied. Finally, field investigations are necessary to further validate the results.

ACKNOWLEDGMENT

This project has received funding from the European Union's Horizon 2020 research and innovation program under the Marie Skłodowska-Curie grant agreement No. 858358 (LIKE – Lidar Knowledge Europe).

REFERENCES

[1] D. Schlipf, *Lidar-Assisted Control Concepts for Wind Turbines*. PhD thesis, University of Stuttgart, 2015.

[2] E. Simley, P. Bortolotti, A. Scholbrock, D. Schlipf, and K. Dykes, "IEA wind task 32 and task 37: Optimizing wind turbines with lidar-assisted control using systems engineering," *Journal of Physics: Conference Series*, vol. 1618, p. 042029, sep 2020.

[3] D. P. Held and J. Mann, "Lidar estimation of rotor-effective wind speed – an experimental comparison," *Wind Energy Science*, vol. 4, no. 3, pp. 421–438, 2019.

[4] E. Simley and L. Pao, "A longitudinal spatial coherence model for wind evolution based on large-eddy simulation," in *2015 American Control Conference (ACC)*, pp. 3708–3714, IEEE, 2015.

[5] Y. Chen, D. Schlipf, and P. W. Cheng, "Parameterization of wind evolution using lidar," *Wind Energy Science*, vol. 6, no. 1, pp. 61–91, 2021.

[6] F. Guo and D. Schlipf, "Lidar wind preview quality estimation for wind turbine control," in *2021 American Control Conference (ACC)*, pp. 552–557, 2021.

[7] A. Sathe, R. Banta, L. Pauscher, K. Vogstad, D. Schlipf, and S. Wylie, "Estimating turbulence statistics and parameters from ground- and nacelle-based lidar measurements," technical report, International Energy Agency, October 2015.

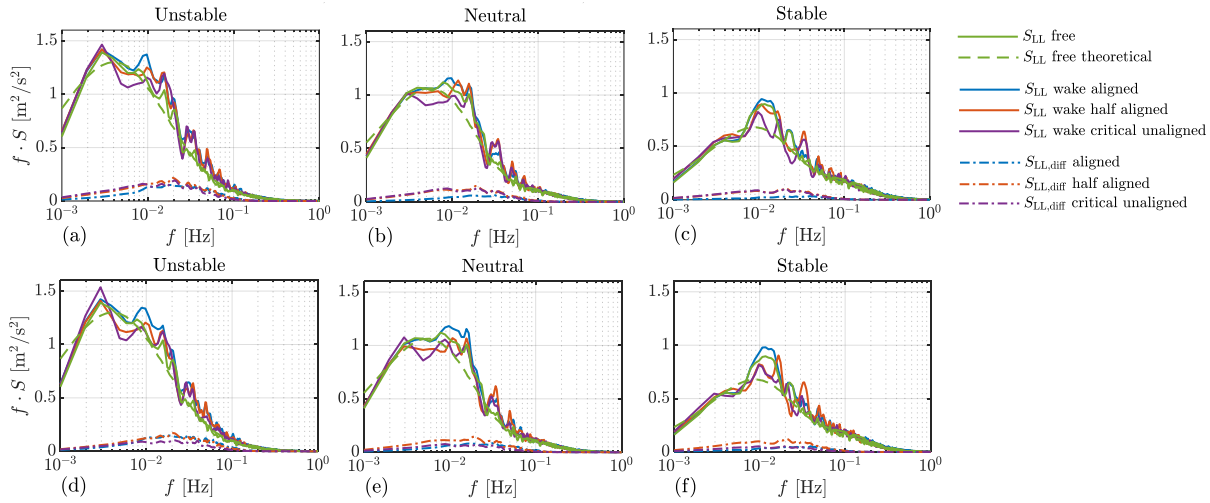

Fig. 6. Comparisons of spectra between the wake included turbulence and the freestream turbulence. "$S_{\mathrm{LL,diff}}$" the auto-spectra of the difference: $u_{\mathrm{L,wake}} - u_{\mathrm{L,free}}$. (a)-(c): the 5D configuration. (d)-(f): the 7D configuration.

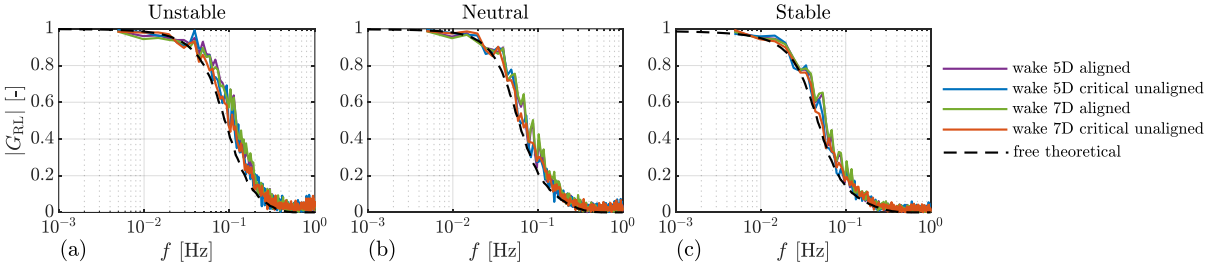

Fig. 7. Comparison of the optimal transfer function gain.

[8] E. Simley, H. Fürst, F. Haizmann, and D. Schlipf, "Optimizing lidars for wind turbine control applications – results from the IEA wind task 32 workshop," *Remote Sensing*, vol. 10, no. 863, 2018.

[9] J. Mann, "The spatial structure of neutral atmospheric surface-layer turbulence," *Journal of Fluid Mechanics*, vol. 273, pp. 141–168, 1994.

[10] J. C. Kaimal, J. C. Wyngaard, Y. Izumi, and O. R. Coté, "Spectral characteristics of surface-layer turbulence," *Quarterly Journal of the Royal Meteorological Society*, vol. 98, no. 417, pp. 563–589, 1972.

[11] IEC 61400-1, *Wind turbines - Part 1: Design requirements*. International Electrotechnical Commission, 2019.

[12] D. Conti, *Wind turbine load validation under wake conditions using Doppler lidar*. PhD thesis, Technical University of Denmark, Denmark, 2020.

[13] J. Mann, "The spatial structure of neutral atmospheric surface-layer turbulence," *Journal of fluid mechanics*, vol. 273, pp. 141–168, 1994.

[14] J. Jonkman, S. Butterfield, W. Musial, and G. Scott, "Definition of a 5-MW reference wind turbine for offshore system development," Tech. Rep. TP-500-38060, NREL, 2009.

[15] A. Peña, "Østerild: A natural laboratory for atmospheric turbulence," *Journal of Renewable and Sustainable Energy*, vol. 11, no. 6, p. 063302, 2019.

[16] J. Mann, "Wind field simulation," *Probabilistic engineering mechanics*, vol. 13, no. 4, pp. 269–282, 1998.

[17] H. A. Madsen, G. C. Larsen, T. J. Larsen, N. Troldborg, and R. Mikkelsen, "Calibration and Validation of the Dynamic Wake Meandering Model for Implementation in an Aeroelastic Code," *Journal of Solar Energy Engineering*, vol. 132, 10 2010. 041014.

[18] J. Jonkman and K. Shaler, "Fast. farm user's guide and theory manual," 2021.

[19] J. Jonkman, P. Doubrawa, N. Hamilton, J. Annoni, and P. Fleming, "Validation of fast. farm against large-eddy simulations," in *Journal of Physics: Conference Series*, vol. 1037, p. 062005, IOP Publishing, 2018.

[20] M. Kretschmer, J. Jonkman, V. Pettas, and P. W. Cheng, "Fast.farm load validation for single wake situations at alpha ventus," *Wind Energy Science Discussions*, vol. 2021, pp. 1–20, 2021.

[21] G. I. Taylor, "The spectrum of turbulence," *Proceedings of the Royal Society of London. Series A - Mathematical and Physical Sciences*, vol. 164, no. 919, pp. 476–490, 1938.

[22] G. C. Larsen, H. A. Madsen, K. Thomsen, and T. J. Larsen, "Wake meandering: a pragmatic approach," *Wind Energy: An International Journal for Progress and Applications in Wind Power Conversion Technology*, vol. 11, no. 4, pp. 377–395, 2008.

[23] D. P. Held and J. Mann, "Lidar estimation of rotor-effective wind speed-an experimental comparison," *Wind Energy Science*, vol. 4, no. 3, pp. 421–438, 2019.

[24] D. Schlipf, J. Mann, and P. W. Cheng, "Model of the correlation between lidar systems and wind turbines for lidar assisted control," *Journal of Atmospheric and Oceanic Technology*, vol. 30, no. 10, pp. 2233–2240, 2013.

[25] D. Schlipf, *Lidar-Assisted Control Concepts for Wind Turbines*. Dissertation, University of Stuttgart, 2015.

[26] E. Simley and L. Pao, "Reducing lidar wind speed measurement error with optimal filtering," in *2013 American Control Conference*, pp. 621–627, 2013.

[27] N. Wiener *et al.*, *Extrapolation, interpolation, and smoothing of stationary time series: with engineering applications*, vol. 8. MIT press Cambridge, MA, 1964.

[28] N. Metropolis and S. Ulam, "The monte carlo method," *Journal of the American Statistical Association*, vol. 44, no. 247, pp. 335–341, 1949. PMID: 18139350.

[29] P. Welch, "The use of fast fourier transform for the estimation of power spectra: a method based on time averaging over short, modified periodograms," *IEEE Transactions on audio and electroacoustics*, vol. 15, no. 2, pp. 70–73, 1967.